Science and Innovation of Advanced Materials

The Materials Research Society of Thailand

Research Article

Biobased Activated Carbon from Palm Biomass Enhancing with Acid Treatment as Supercapacitor Electrode Material

Vituruch Goodwin*, Thanathon Sesuk, Parinya Jitreewas

National Energy Technology Center (ENTEC), National Science and Technology Development Agency (NSTDA), Pathum Thani 12120, Thailand

* Corresponding author e-mail: vituruch.goo@entec.or.th

Received: *February 28th, 2024* | ***Revised:*** *April 10th, 2024* | ***Accepted:*** *April 13th, 2024*

Abstract: Current research on energy storage systems, batteries, and supercapacitor devices is aimed to enhance efficiency and improve environmental sustainability. Supercapacitors offer remarkable attributes such as high transient response and power density. Typically, supercapacitor electrode is made from highly porous carbon material, activated carbon. Commercial activated carbon could be produced from coal, peat, or coconut shell. This study focused on utilization of palm biomass, palm empty fruit bunch (EFB), as raw material to produce activated carbon electrode. The highly porous activated carbon from EFB was synthesized via a low-temperature hydrothermal process and chemical activation. The resulting EFB activated carbon demonstrates favorable characteristics in terms of elevated surface area and porosity. This research investigates the enhancement of activated carbon with acid treatment during hydrothermal process. Two types of acid, citric acid, and phosphoric acid, at different concentrations, were added to biomass. The acid-treated activated carbon from palm biomass was characterized for the specific surface area (BET), pore size distribution and pore volume using the N_2 adsorption/desorption technique. The acid-treated activated carbon was fabricated into carbon electrodes and assembled in a symmetrical supercapacitor with 1M H_2SO_4 as an electrolyte. The supercapacitor performance of acid-treated activated carbon was tested in a symmetrical Swagelok cell to assess specific capacitance using cyclic voltammetry and galvanostatic charge-discharge methods. The acid-treated activated carbon has higher specific capacitance than the activated carbon without acid treatment. This superior performance is attributed to the reduced internal resistance as revealed by the Electrochemical Impedance Spectroscopy (EIS) result. This is possibly due to the formation of micropores in the range of 0.6–0.7 nm which is a suitable pore size for ion transportation in H_2SO_4 electrolytes. This research has shown that biobased activated carbon from palm oil biomass with acid treatment has a high potential to be used as supercapacitor electrode material.

Keywords: Activated carbon, Palm biomass, Hydrothermal, Energy storage, Supercapacitor

1. Introduction

Over the years, the growing demands for efficient utilization of renewable energy resources for sustainable development have become extremely urgent and important [1,2]. Supercapacitors, as energy storage devices widely used to be equipped with renewable energy production systems such as solar or wind electrical generators, have been a popular research topic because of their excellent electrochemical properties. Electrochemical double-layer capacitors

* The work was presented at The 22nd International Symposium on Eco-materials Processing and Design (ISEPD 2024), 21-24 January 2024

(EDLCs) or supercapacitors have high power density, fast charge/discharge rate, and excellent cycle stability [3,4]. Researchers around the world are trying to explore and develop high performance electrode of supercapacitors which plays an important role in energy storage [5–7]. Limited fossil resources and environmental problems have driven the utilization of biobased activated carbon from renewable lignocellulosic biomass with the development of biorefinery techniques to decrease or eliminate the reliance on fossil resources [8–10].

Many efforts have been made to develop biobased activated carbon supercapacitor materials with high capacitance and excellent cycle stability. Various biomass-derived activated carbon materials are promising candidates for supercapacitors [11,12] since they possess a large specific surface area [13], are renewable, and have a low cost compared with graphene or carbon nanotubes [14,15]. Agricultural residues such as rice straw [16], soybean [17], coffee grinds [18], palm empty fruit bunch [19–22], banana fiber [23], corn residues [24–26], sugarcane bagasse [27,28], and coconut coir pith [29] are examples of biomass which previously have been prepared and studied for supercapacitor application. In Thailand, the palm oil industry has generated a large amount of biomass waste. Palm empty fruit bunches (EFB) are the most underutilized waste products; therefore, in this study, we aim to increase their value through the hydrothermal carbonization process (HTC) to produce high-value activated carbon materials [30–33]. The advantages of the hydrothermal carbonization process are low-temperature process and environmentally friendly [13,34]. Hydrothermal carbonization is usually performed in water in the temperature range of 120–260 °C for several hours under saturated pressure, which will reduce the dielectric constant of water and turn it into a suitable solvent for non-polar substances. Adding acid-base catalyzed reactions can facilitate biomass to undergo thermal degradation in water. Adding acid during the HTC could assist in the transformation of carbohydrates and/or biomass into functional hydrochar [35–37]. Recently, Song et al. reported that citric acid and lignocelluloses on the hydroxyl (-OH) groups readily undergo esterification under a specific condition. Thus, the esterification reactions between citric acid and lignin could prevent the formation of reactive intermediate and thus suppress lignin repolymerization [38]. Barakat et al. reported that phosphoric acid is an efficient activating agent to improve the properties of carbon-based materials before and/or after carbonization [39]. A suitable quantity of protons might promote the formation of acidic surface oxygen-containing functional groups (OFG), which was the dominant influence parameter to enhance the surface properties of activated carbon after chemical activation [40].

To enhance the surface area and surface properties of biobased activated carbon, which plays an important role in electrical capacitance, the acid addition to treat the biomass during hydrothermal carbonization was studied. In this work, the acid-treated hydrothermal carbonization process was performed using two different acids, i.e., citric acid and phosphoric acid. These acids were added at different concentrations to EFB biomass during the hydrothermal process. The potassium hydroxide (KOH) activation process was performed under a carbon dioxide atmosphere in the tube furnace at 700 °C. The acid-treated activated carbon was fabricated into carbon electrodes and assembled in a symmetrical supercapacitor with 1M H_2SO_4 as an electrolyte. The supercapacitor performance of acid-treated activated carbon was tested in a symmetrical Swagelok cell to assess specific capacitance using a galvanostatic charge-discharge method, and the specific capacitance values (C_{sp}, $F \cdot g^{-1}$) were calculated from the discharge curve. The effect of different acid treatments on the EFB-activated carbon chemical and surface properties was also reported.

2. Methodology

2.1 Preparation of EFB-activated carbon with and without acid treatment

The biomass from the palm empty fruit bunch (EFB) used in this study was collected from a palm oil plantation in Pathum Thani province, Thailand. The preparation of EFB biomass was done in the following order. First, the EFB was chopped into small pieces, washed with tap water, and dried under the sunlight for 3 days. Then the EFB pieces were rinsed with tap water to remove any impurities and dried in a hot air oven at 110 °C overnight. After oven-drying, the EFB was ground with a grinding machine (WF-10B, Thaigrinder) and sequentially sieved for sizes 75–150 μm to obtain the EFB powder. The activated carbon from EFB was synthesized via hydrothermal carbonization and

chemical activation. The hydrothermal process was performed in a high-pressure autoclave reactor (Parr Instrument) using 30 g of EFB powder and 250 ml of DI water. The hydrothermal carbonization condition was at 200 °C for 2 h to obtain the untreated EFB hydrochar. While the citric acid or phosphoric-treated active carbon was prepared by adding 0.5, 1, or 10 wt% of acid to EFB powder during the hydrothermal step. The hydrochar was then washed with DI water until the rinsed water reached pH 7 and then dried in a hot oven at 110 °C for 48 h. The solid hydrochar was followed by a chemical activation process using KOH as an activating agent at 2:1 ratio by weight of KOH:hydrochar and activated in the tube furnace using ramp rate at 5 °C·min^{-1} until reaching the activating temperature at 700 °C, then activated under CO_2 atmosphere for 2 h. After activation, the EFB-activated carbon with and without acid treatment was washed with HCl solution, DI water, NaOH solution, and DI water in the final step. In the end, EFB-activated carbon was dried at 110 °C for 16 h before further use for any characterization and electrochemical performance tests. The EFB-activated carbon without acid treatment is denoted as EFB-HW. The citric acid-treated EFB-activated carbon samples are abbreviated as EFB-HCxx, and the phosphoric acid-treated EFB-activated carbon samples are abbreviated as EFB-HPxx where xx is the concentration of the acid added during the hydrothermal step for each sample.

2.2 Characterization

The specific surface area of EFB-activated carbon was evaluated by the Brunauer-Emmett-Teller (BET) theory using the physical adsorption of nitrogen (ASAP 2460, Micromeritics Instrument Corporation). The nitrogen physisorption data were calculated to determine the specific surface area (SSA), and the pore volume and pore size distribution were determined from the data using non-local density functional theory (NLDFT). The structure of EFB-activated carbon was investigated using X-ray diffraction (XRD, TTRAX-III, Rigaku Corporation). The XRD patterns were recorded with Cu Kα1 radiation at 50 kV and 300 mA, 10°–80° 2θ, 0.02° step size, and 2.33°/min scan speed. The surface elemental compositions and carbon species characterization of EFB-activated carbon samples were analyzed using X-ray photoelectron spectroscopy (XPS, Kratos Axis Ultra DLD with Al Kα radiation). The EFB hydrochar samples with and without acid treatment were collected after the hydrothermal process at 200 °C for 2 h and were analyzed by Infrared Fourier Transform spectroscopy (FT-IR). The spectra were collected using an FT-IR spectrometer coupled with an MCT-A detector (Nicolet iS50, Thermo Fisher Scientific Inc.).

2.3 Electrochemical measurements

The EFB-activated carbon samples were electrochemically tested using a symmetrical cell (Swagelok cell). The carbon electrode was prepared by mixing EFB-activated carbon, conductive carbon (Carbon black; Li-100), and binder (12 wt% polyvinylidene difluoride (PVDF) in N-methyl-2-pyrrolidone (NMP)) at the ratio of 8:1:1 by weight using a planetary mixer at 1200 rpm for 10 min. The carbon slurry was cast on a current collector (stainless foil, thickness 0.01 mm) and dried in a vacuum oven at 80 °C for 24 h. The dried electrode was cut into a circle with 11 mm diameter and assembled with a nonwoven glass fiber (Whatman GF/F, Sigma-Aldrich) as a separator and 1M H_2SO_4 solution as the electrolyte.

The EFB-activated carbon was electrochemically tested for supercapacitor performance using Galvanostatic charge-discharge measurement (GCD) performed at a currents range of 0.1 to 2 A·g^{-1} with cut-off potentials from 0.0 to 0.6 V (Maccor 4000 battery analyzer). The specific capacitance value (C_{sp}, F·g^{-1}) was calculated from the discharge curve using Equation (1)

$$C_{sp} = \frac{4I\Delta t}{\Delta V m} \quad (1)$$

where I (A) is the discharge current, Δt (s) is the discharge time, ΔV (V) is the potential drop during discharge, and m (g) is the mass of the active material in both electrodes. The cyclic voltammetry (CV) measurement was performed between -0.2 and 1.0 V using potential scan rates 10 mV·s^{-1} and a step size of 0.5 mV. The internal resistance of the

supercapacitor cell was evaluated from Electrochemical Impedance Spectroscopy (EIS) measurement carried out in the frequency range of 10^{-2}–10^{5} Hz using an Autolab PGSTAT204 potentiostat/galvanostat.

3. Results and discussion

The preparation process of EFB-activated carbon includes three main steps: hydrothermal carbonization (HTC), KOH chemical activation, and washing of impurities. In this study, both the KOH and the activated temperature, which play an important role in the generation of the pore structure of activated carbon, were fixed. The condition using an activation weight ratio (KOH:hydrochar) of 2:1 with carbonization at 700 °C was selected as the optimal condition to produce EFB-activated carbon for supercapacitor applications.

3.1 Characterization of hydrochar and EFB-activated carbon

The EFB biomass and hydrochar of EFB-HW, EFB-HCxx, and EFB-HPxx were analyzed for chemical properties using FT-IR. The FT-IR fingerprints of EFB biomass and EFB hydrochar with and without acid treatment are shown in Figures 1(a) and 1(b). After the HTC process, the oxygen-containing functional groups (OFG) were slightly formed on hydrochar without acid treatment (HC-HW) compared to the original EFB biomass. With citric acid treatment, the oxygen-containing functional groups (OFG) were primarily formed, which displayed in FT-IR spectra as very large peaks of O-H stretching at 3340 cm^{-1} in carboxyl groups [41] and a C-O stretching at 1030 cm^{-1} [41,42] (Figure 1(a)) compared to hydrochar without acid treatment (HC-HW). The C-O bond could represent a variety of oxygen-containing functional groups, including acidic carboxyl, anhydrides, lactones, and phenols. Basic oxygen-containing functional groups include quinone, chromene, and pyrone, while neutral groups are carbonyl and ether [43]. The higher concentration of citric acid influences the formation of more OFG. While in the phosphoric acid treatment cases, HC-HPxx hydrochar displays similar FT-IR spectra to non-acid-treated HC-HW. Thus, the addition of citric acid has a dominant effect during the hydrothermal carbonization of EFB. The XRD patterns of all EFB-activated carbon samples are shown in Figures 1(c) and 1(d). The XRD patterns of all the samples exhibit the amorphous structure of carbon. The XRD results show no significant difference in crystal structure among the activated carbon samples prepared with citric acid or phosphoric acid treatment in this study. All samples display the XRD broad peaks at 2θ around 24° and 44°, which correspond to the (200) and (101) phases of carbon (JCPDS: 10-0425). The large signal intensity in the low-angle region, especially in EFB-HC0.5, indicates high porosity within the samples [44].

The BET-specific surface area and pore volume of all EFB-activated carbon samples are summarized in Table 1. The specific surface area of non-acid-treated carbon, EFB-HW, is 1894 $m^2 \cdot g^{-1}$. The citric acid-treated carbons have a lower surface area than EFB-HW at 1505, 1487 and 1615 $m^2 \cdot g^{-1}$. All EFB-activated carbon in this study has a high surface area comparable to commercial carbon, YP50F, with a surface area of 1654 $m^2 \cdot g^{-1}$. The mesopore percentage of citric acid-treated carbon has decreased from 18.8% to 3.4, 4.9, and 12.5%. The higher the citric acid concentration, the higher the mesopore. This could be related to the high oxygen-containing groups (OFG) found after hydrothermal process. The OFG could affect the pore formation which leads to lower surface area and lower mesopores. Conversely, the phosphoric acid-treated carbons have slightly lower surface area than EFB-HW at 1610, 1792, and 1832 $m^2 \cdot g^{-1}$. In contrast, the mesopore percentage differs slightly from the non-acid-treated carbon, EFB-HW. This indicates that phosphoric acid treatment has no significant effect on the pore generation process during KOH activation. Similar chemical functional groups of hydrochar, i.e., no increase in OFG with phosphoric acid treatment, suggesting that OFG plays an important role in KOH activation process, hence similar pore properties were found among HC-HW and HC-HPxx samples.

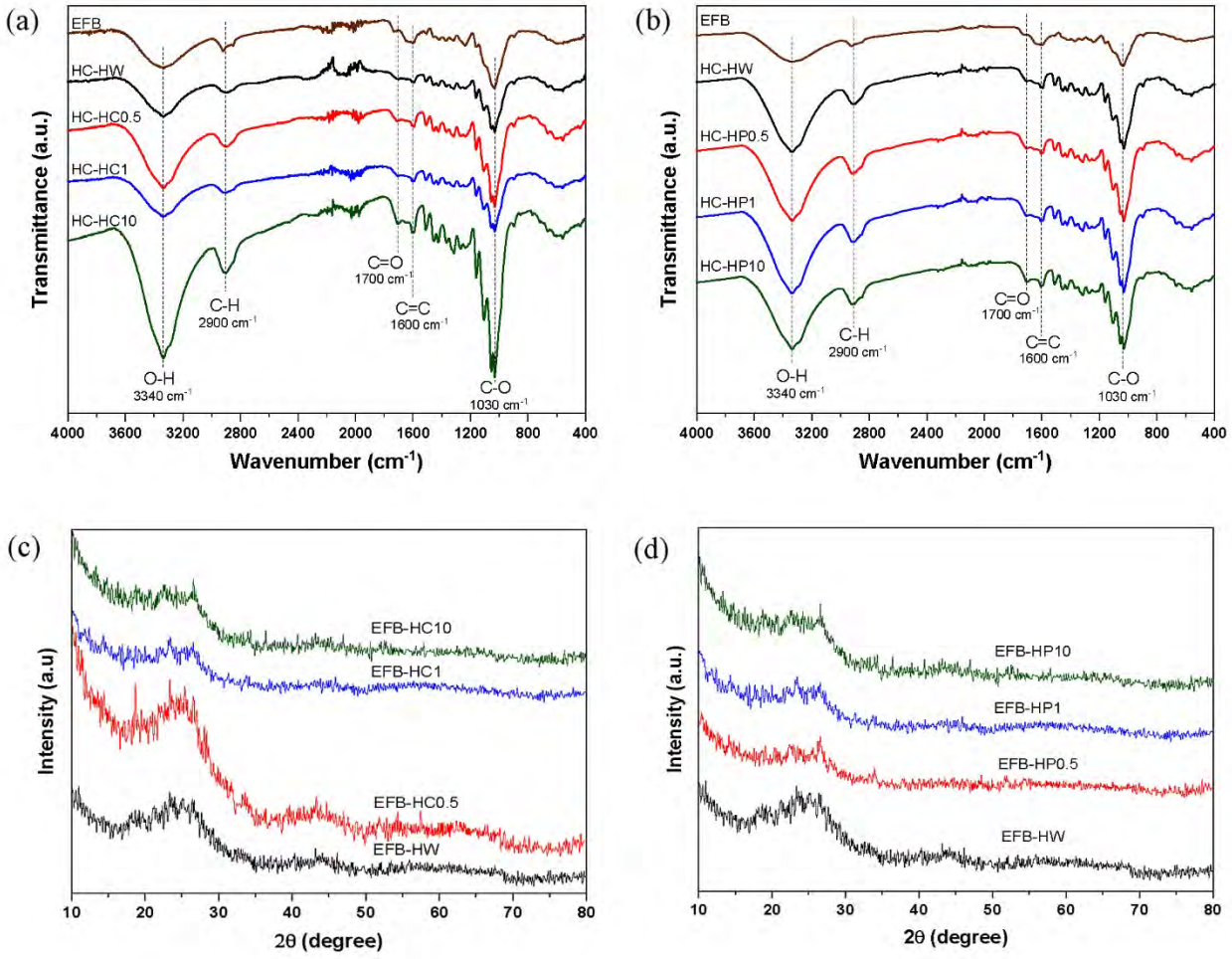

Figure 1 (a) FTIR spectra of EFB biomass, hydrochar HC-HW and hydrochar samples with citric acid treatment, HC-HCxx, (b) FTIR spectra of EFB biomass, hydrochar HC-HW and hydrochar samples with phosphoric acid treatment, HC-HPxx, (c) XRD patterns of activated carbon, EFB-HW and AC with citric acid treatment EFB-HCxx, and (d) XRD patterns of activated carbon, EFB-HW and AC with phosphoric acid treatment EFB-HPxx.

Table 1 BET Surface area and pore volume of EFB-activated carbon produced without acid treatment (EFB-HW) and with acid treatment during the hydrothermal process (EFB-HCxx and EFB-HPxx)

Activated carbon	Surface Area ($m^2 \cdot g^{-1}$)	Mesopore (%)	Total pore volume ($cm^3 \cdot g^{-1}$)	Micropore volume ($cm^3 \cdot g^{-1}$)	Mesopore volume ($cm^3 \cdot g^{-1}$)
EFB-HW	1894	18.8	0.87	0.71	0.16
EFB-HC0.5	1505	3.4	0.60	0.58	0.02
EFB-HC1	1487	4.9	0.61	0.58	0.03
EFB-HC10	1615	12.5	0.75	0.66	0.09
EFB-HP0.5	1610	25.8	0.82	0.61	0.21
EFB-HP1	1792	18.1	0.85	0.69	0.15
EFB-HP10	1832	17.8	0.90	0.74	0.16

The N_2 adsorption-desorption isotherms of all EFB-activated carbon samples are shown in Figures 2(a) and 2(c). All AC samples exhibit the typical IV isotherms with hysteresis loops associated with slit-shaped pores [45]. The pore size distribution plot (PSD) of all EFB-activated carbon samples is generated using density functional theory (DFT), which in the refined form of nonlocal density functional theory (NLDFT), where the pores of different sizes are assumed to be all the same regular shape (e.g., cylinders or slits). Generally, each pore is assumed to behave independently [46]. The PSD plot of citric acid-treated carbon is shown in Figure 2(b), and the PSD plot of phosphoric acid-treated carbon is shown in Figure 2(d). EFB-activated carbon with 0.5 and 1 wt% citric acid treatment contain large amount of micropore in the size of 0.6–0.7 nm. It has significant increases in the micropore percentage of these samples. However, EFB-HPxx samples with phosphoric acid treatment have no significant change in pore size distribution. The PSD plot of non-acid-treated samples and EFB-HPxx contain both micropores and mesopores in their structure. This indicates that phosphoric acid treatment has no significant effect on pore generation.

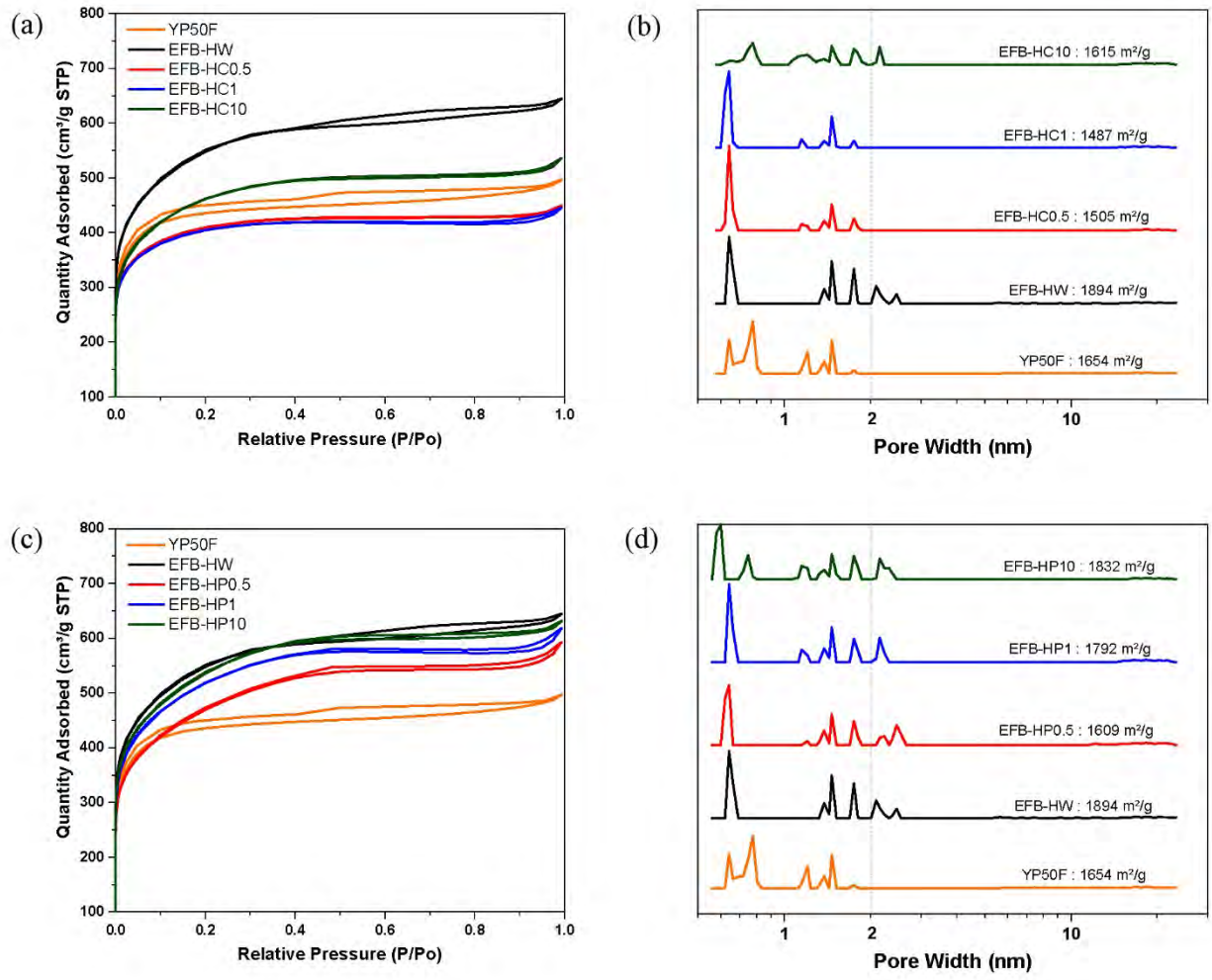

Figure 2 (a) N_2 adsorption-desorption isotherms of EFB-HW, AC with citric acid treatment, EFB-HCxx, and YP50F, (b) PSD plots of EFB-HW, AC with citric acid treatment, EFB-HCxx, and YP50F, (c) N_2 adsorption-desorption isotherms of EFB-HW, AC with phosphoric acid treatment, EFB-HPxx, and YP50F, and (d) PSD plots of EFB-HW, AC with phosphoric acid treatment, EFB-HPxx, and YP50F.

The surface chemistry of EFB-activated carbon samples was investigated using XPS analysis. As shown in Figure 3(a), the C1s analysis of non-acid-treated carbon exhibits three peaks ascribed to C-C (285.5 eV), O-C-O (287.1 eV), and C=O (288.3 eV) in the XPS elemental analysis mode. According to the XPS spectrum of citric acid-treated carbons (Figure 3(b–d)), we find that the C1s spectrum can be divided into four separate peaks attributed to sp2 & sp3 C-C (284.7–285.2 eV), C–O (286.5–287 eV), C=O (287.2–289 eV), and O-C=O (289.2–290.7 eV), respectively [46–49]. It is clearly seen that citric acid treatment can introduce more OFG to the EFB-activated carbon.

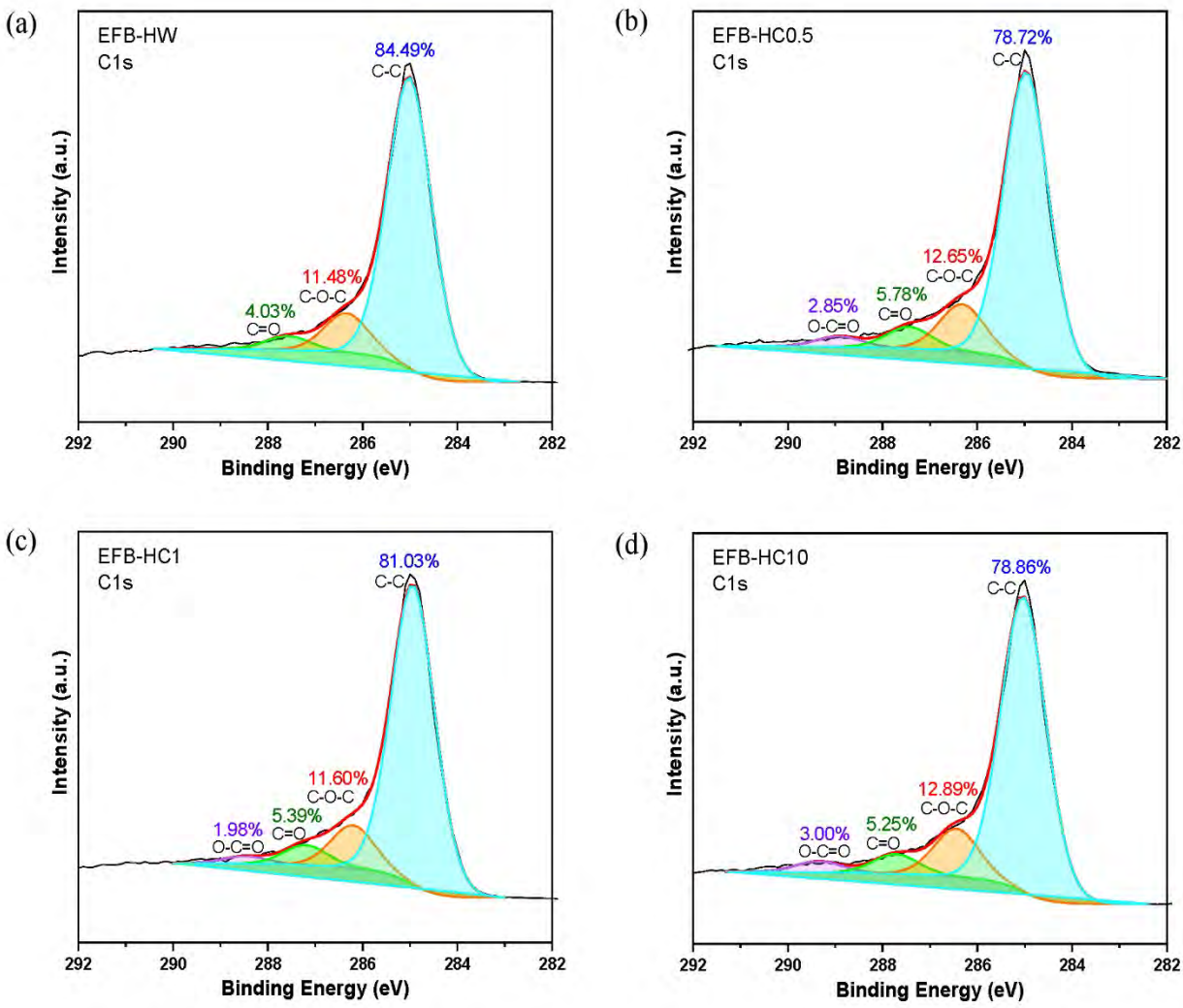

Figure 3 XPS elemental analysis C1s of (a) EFB-HW, and citric acid-treated carbons, (b) EFB-HC0.5, (c) EFB-HC1, and (d) EFB-HC10.

A similar XPS elemental analysis spectra of phosphoric acid are displayed in Figure 4 (b–d). The C1s spectrum also shows four separate peaks attributed to C-C, C-O, C=O, and O-C=O functional groups. Thus, both citric and phosphoric acid treatment during hydrothermal carbonization has introduced carboxyl groups on the surface of EFB-activated carbon. This is further confirmed that the acid-treated EFB-activated carbon contains more OFG-like carboxyl, which can improve the wettability of the carbon electrode, allowing the ions to enter the pores of the material more easily [50,51].

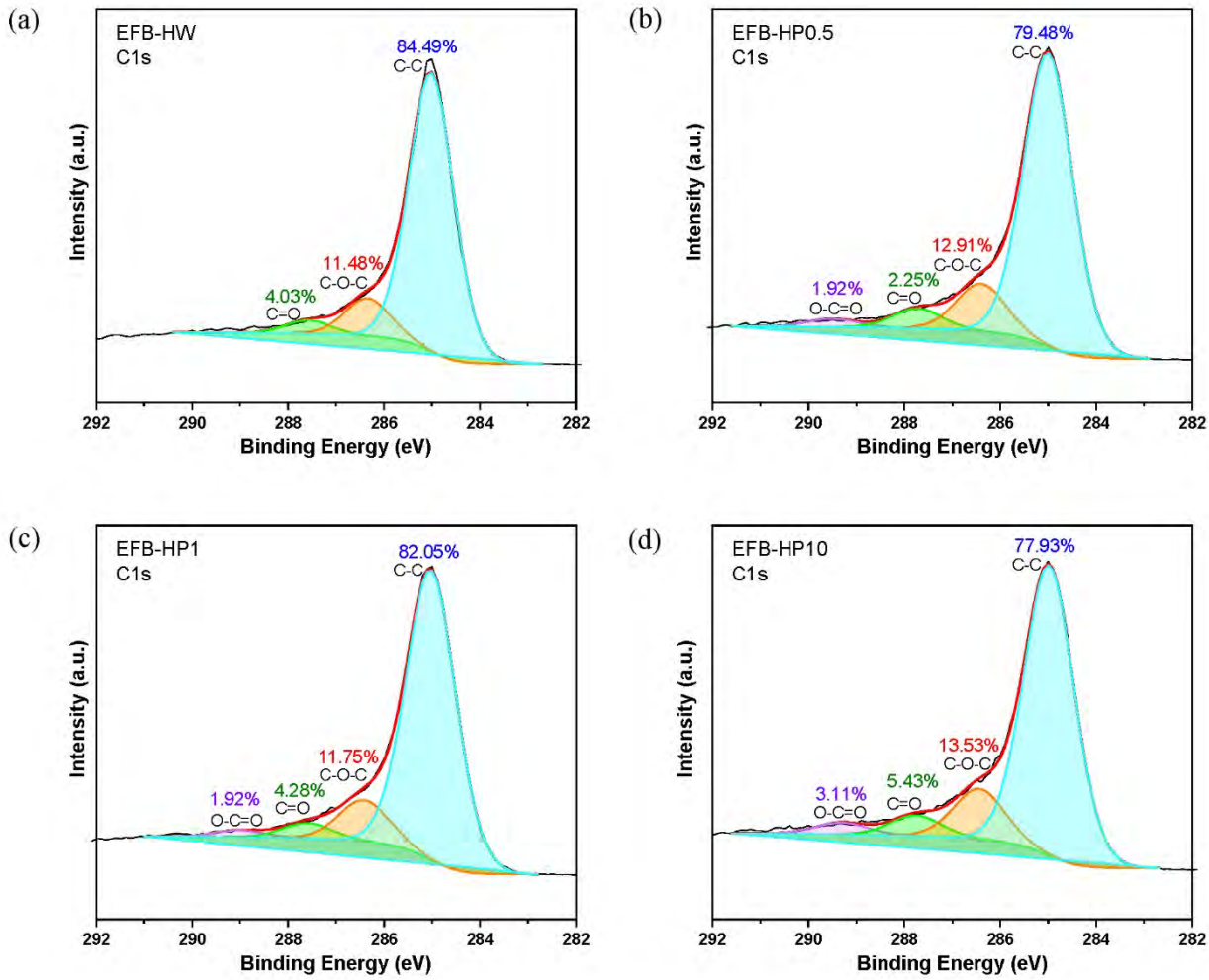

Figure 4 XPS elemental analysis C1s of (a) EFB-HW, and phosphoric acid-treated carbons, (b) EFB-HP0.5, (c) EFB-HP1, and (d) EFB-HP10.

3.2 Electrochemical performance

The advantage of the high surface area of the prepared EFB-activated carbon, with its highly porous structure and oxygen-containing functional groups, is a suitable candidate for high performance supercapacitor electrode material. The following electrochemical performance tests were performed to evaluate supercapacitor performance including GCD rate test at various current densities, CV measurement, and EIS test. All electrochemical tests were performed in the two-electrode Swagelok cell. Figures 5(a) and 6(a) display the charge-discharge curves of EFB-activated carbon with and without acid treatment. The charge-discharge curves of all EFB-activated carbon have a regular triangular shape representing the high electrochemical reversibility and coulombic efficiency according to supercapacitor behavior. The results of GCD tests investigated at various current densities are shown in Figures 5(b) and 6(b). The gravimetric specific capacitance of citric acid-treated samples is higher than the non-acid-treated sample (EFB-HW) and commercial carbon (YP50F) reported at 143.8, 134.6, and 125.6 $F{\cdot}g^{-1}$ at a current density of 0.1 $A{\cdot}g^{-1}$, for EFB-HC0.5, EFB-HC1, and EFB-HC10, respectively. The gravimetric specific capacitance of phosphoric acid-treated samples is in the same range or slightly lower when compared with the non-acid-treated sample (EFB-HW) reported at 110.1 $F{\cdot}g^{-1}$ at a current density of 0.1 $A{\cdot}g^{-1}$. However, all the EFB-activated carbon samples prepared in this study

show higher capacitance than commercial carbon, YP50F, with a C_{sp} of 71.6 F·g^{-1} at a current density of 0.1 A·g^{-1}. Figures 5(c) and 6(c) display the CV curves of all the EFB-activated carbon samples. The shape of the CV curves maintains an almost symmetric quasi-rectangular shape, indicating the EFB-activated carbon exhibits excellent electrochemical capacitive behavior. Both citric acid and phosphoric acid-treated carbons display a small redox peak on the CV curve, demonstrating that the total capacitance of the materials could result from a combination of double-layer capacitance and pseudocapacitance. As shown in Figure 5(c), the CV curve of EFB-HC0.5 has the largest quasi-rectangular area, and the GCD curve also shows that EFB-HC0.5 has the longest charge/discharge time, which indicates that EFB-HC0.5 has the best electric energy storage capacity. The EIS (Electrochemical Impedance Spectroscopy) Nyquist plots of citric acid-treated carbons are presented in Figure 5(d). The semicircle observed at the high-frequency region corresponds to the electron-transfer-limited process. At the same time, the linear portion in the low-frequency range characterizes the diffusion-limited electron-transfer process [52,53]. The semicircular diameter reflects the charge transfer resistance at the electrode/electrolyte interface. Citric acid-treated carbons, EFB-HC.5, and EFB-HC1, show low resistance, Rp, (Table 2) calculated from semicircle diameters, representing low charge transfer resistance, which indicates good conductivity and ion diffusion into pores. This confirmed the effect of OFG added on the carbon surface via citric acid treatment, as well as the influence of increased wettability between the carbon surface and electrolyte. At the low frequency, the charge transfer is fast, and ionic diffusion is limited within this region, EFB-HC0.5, which has a lower content of mesopores, show slightly decrease in slope of this linear region representing the limitation of ion transportation from the electrolyte into micropores. The calculation of resistance from the Nyquist plot (Figure 5(d)) is displayed in Table 2.

Table 2 Resistance from EIS and Nyquist plot data of EFB-activated carbon produced without acid treatment (EFB-HW) and with acid treatment during the hydrothermal process (EFB-HCxx and EFB-HPxx)

Activated carbon	Rp (Ω)	Rs (Ω)	CPE
EFB-HW	26.33	1.36	0.74
EFB-HC0.5	8.13	0.70	0.82
EFB-HC1	13.49	1.08	0.85
EFB-HC10	30.87	0.29	0.77
EFB-HP0.5	50.08	8.78	0.84
EFB-HP1	25.68	1.14	0.85
EFB-HP10	16.46	0.79	0.80

In Table 2, Rs is the sum of the resistances of the bulk electrolyte and the electrode, or the solution resistance is calculated from the equivalent series resistance (ESR) model shown in Figure 5(e). Rp symbolizes the charge transfer resistance, which is depicted as the diameter of the semicircle, signifies the ions resistance as they move through electrolyte within the pores of the carbon electrodes. The Citric acid-treated carbons, EFB-HC.5, and EFB-HC1, exhibit low Rp, therefore represent high conductivity. CPE stands for Constant Phase Element, which is often used to represent the behavior of double layer capacitance in EIS. It characterizes the capacitance of the electrical double layer formed at the electrode-electrolyte interface.

However, the EIS Nyquist plots of phosphoric acid-treated carbons, presented in Figure 6(d), have not improved wettability or ion diffusion. This result indicates that the optimal OFG on the carbon surface is necessary. Considering the increase of internal resistance in phosphoric acid-treated samples, the importance of pore size distribution must be reviewed. The phosphoric acid-treated has a high mesopores percentage similar to the non-acid-treated-carbons, EFB-HW. Thus, the ion diffusion through pores must be the same behavior. The increased internal resistance could be caused by the acid oxygen in functional groups that hinder the diffusion of acid electrolytes. Contrary to the citric acid-treated carbons, which contain the majority of micropores of 0.6–0.7 nm diameter. This

micropore has a suitable size for storing protons from acid electrolytes, thus resulting in the high electric capacity of EFB-HC0.5 and EFB-HC1 samples.

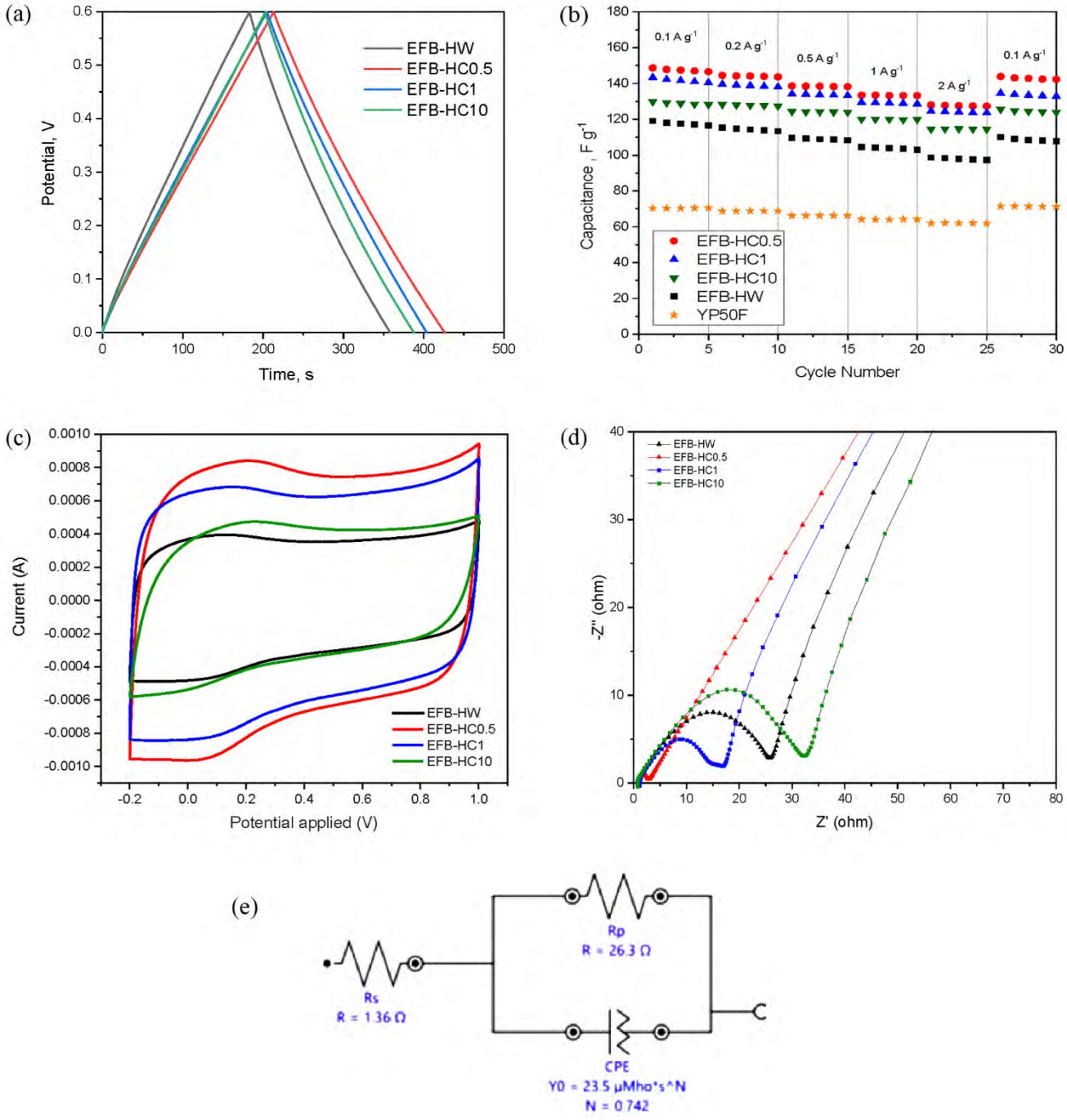

Figure 5 Electrochemical test results of EFB-HW and citric acid-treated carbons; (a) Charge-discharge curve from GCD test, (b) C_{sp} calculated from discharge curve of GCD rate test, (c) CV results, and (d) EIS Nyquist plot, with the equivalent series resistance (ESR) model shown in (e).

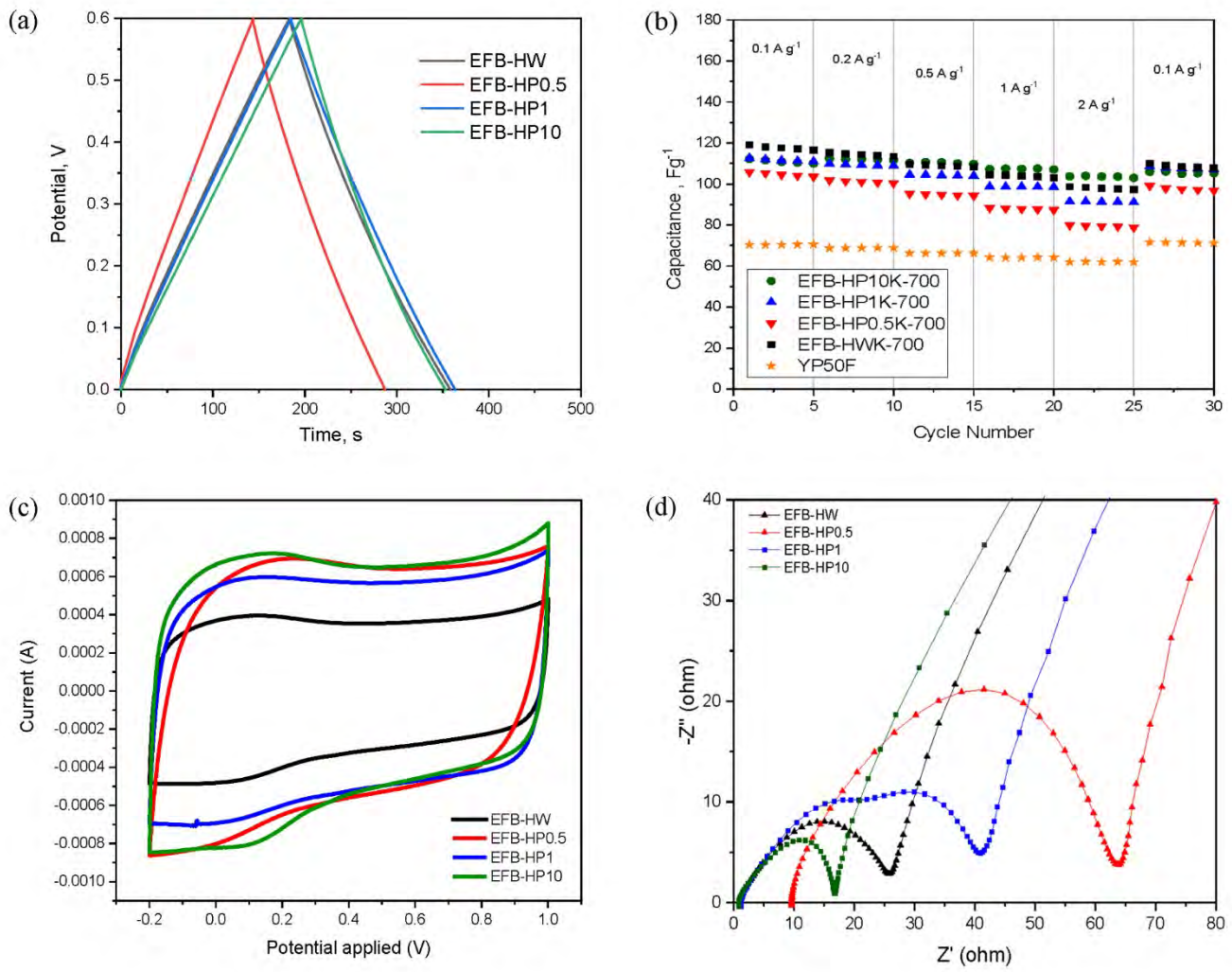

Figure 6 Electrochemical test results of EFB-HW and phosphoric acid-treated carbons; (a) Charge-discharge curve from GCD test, (b) C_{sp} calculated from discharge curve of GCD rate test, (c) CV results, and (d) EIS Nyquist plot.

4. Conclusion

The biobased activated carbon for high-performance supercapacitors application synthesized via the proposed acid treatment hydrothermal carbonization processes was successfully produced from palm empty fruit bunch (EFB) biomass. A specific capacitance value of 143.8 $F{\cdot}g^{-1}$ was obtained at 0.1 $A{\cdot}g^{-1}$ from citric acid-treated EFB carbon. The interconnected micropore structure of EFB-HC0.5 contributed to its high supercapacitive performance by fully utilizing micropores with suitable pore-sized diameters to store ions from acid electrolytes. The citric acid treatment is also favorable to increasing oxygen-containing groups (OFG) on hydrochar and optimizing the pore size distribution (PSD), leading to an excellent electrochemical performance of final activated carbon products. The optimized PSD and OFG on the carbon surface positively reduce internal resistance between electrode/electrolyte interfaces in the aqueous supercapacitor cell. In this study, both citric and phosphoric acid treatment in the hydrothermal process contributed to the addition of OFG, which could enhance the surface wettability and electronic conductivity of biobased activated carbon electrodes. Only the hydrochar synthesized by the citric acid treatment HTC method exhibits high OFG, thus affecting the pore generation process. While the hydrochar synthesized by the phosphoric

acid treatment HTC does not exhibit significant changes in OFG, the resulting activated carbon has a PSD similar to the non-acid-treated carbon. The supercapacitor performance of biobased carbon electrodes is affected by many properties of carbon electrode materials, including surface area, PSD, OFG, micropore and mesopore percentage, etc. The complex mechanism of ion storage in supercapacitors is still an ongoing discussion. This study deduces that the surface properties and optimal pore size are crucial to the ion diffusion and capacitance value. When benchmarked with commercial carbon, the prepared biobased activate carbons from EFB have shown good supercapacitive performance with high specific capacitance. This work not only studies the effect of the citric or phosphoric acid treatment on the EFB hydrochar and activated carbon properties but also successfully converts an underutilized EFB biomass into activated carbon materials with excellent energy storage performance.

Acknowledgment

This work was supported by the National Energy Technology Center, National Science and Technology Development Agency [grant number P-20-51394]. The authors would like to express their appreciations to the Japan-ASEAN Science, Technology and Innovation Platform on Energy and Environment (JASTIP) program for the continual supports of information and collaboration with Kyoto University, Japan.

References

[1] L. Dai, D. W. Chang, J. B. Baek, W. Lu, Carbon nanomaterials for advanced energy conversion and storage, *Small* **8** (2012) 1130-1166.

[2] H. Jiang, P. S. Lee, C. Li, 3D carbon based nanostructures for advanced supercapacitors, *Energ. Environ. Sci.* **6** (2013) 41-53.

[3] A. Burke, Ultracapacitors: Why, how, and where is the technology, *J. Power Sources* **91** (2000) 37-50.

[4] Z. Niu, H. Dong, B. Zhu, J. Li, H. H. Hng, W. Zhou, X. Chen, S. Xie, Highly stretchable, integrated supercapacitors based on single-walled carbon nanotube films with continuous reticulate architecture, *Adv. Mater.* **25** (2013) 1058-1064.

[5] B. Yan, J. Zheng, F. Wang, L. Zhao, Q. Zhang, W. Xu, S. He, Review on porous carbon materials engineered by ZnO templates: Design, synthesis and capacitance performance, *Mater. Des.* **201** (2021) 109518.

[6] M. Tebyetekerwa, I. Marriam, Z. Xu, S. Yang, H. Zhang, F. Zabihi, R. Jose, S. Peng, M. Zhu, S. Ramakrishna, Critical insight: Challenges and requirements of fibre electrodes for wearable electrochemical energy storage, *Energy Environ. Sci.* **12** (2019) 2148-2160.

[7] J. Yan, L. Miao, H. Duan, D. Zhu, Y. Lv, W. Xiong, L. Li, L. Gan, M. Liu, Core-shell hierarchical porous carbon spheres with N/O doping for efficient energy storage, *Electrochim. Acta* **358** (2020) 136899.

[8] A. Bichot, J. P. Delgenès, V. Mèchin, H. Carrère, N. Bernet, D. García-Bernet, Understanding biomass recalcitrance in grasses for their efficient utilization as biorefinery feedstock, *Rev. Environ. Sci. Biotechnol.* **17** (2018) 707-748.

[9] A. Ramos, E. Monteiro, A. Rouboa, Biomass pre-treatment techniques for the production of biofuels using thermal conversion methods-a review, *Energ. Convers. Manag.* **270** (2022) 116271.

[10] L. Zhao, J. Zhang, D. Zhao, L. Jia, B. Qin, X. Cao, L. Zang, F. Lu, F. Liu, Biological degradation of lignin: A critical review on progress and perspectives, *Ind. Crop Prod.* **188** (2022) 115715.

[11] H. Lu, X. S. Zhao, Biomass-derived carbon electrode materials for supercapacitors, *Sustain. Energ. Fuels* **1** (2017) 1265-1281.

[12] A. M. Abioye, F. N. Ani, Recent development in the production of activated carbon electrodes from agricultural waste biomass for supercapacitors: a review, *Renew. Sust. Energ. Rev.* **52** (2015) 1282-1293.

[13] R. F. Susanti, A. A. Arie, H. Kristianto, M. Erico, G. Kevin, H. Devianto, Activated carbon from citric acid catalyzed hydrothermal carbonization and chemical activation of salacca peel as potential electrode for lithium ion capacitor's cathode, *Ionics* **25** (2019) 3915-3925.

[14] Y. B. Tan, J.-M. Lee, Graphene for supercapacitor applications, *J. Mater. Chem. A* **1** (2013) 14814.
[15] H. Zhang, H. Su, L. Zhang, B. Zhang, F. Chun, X. Chu, W. He, W. Yang, Flexible supercapacitors with high areal capacitance based on hierarchical carbon tubular nanostructures, *J. Power Sources* **331** (2016) 332-339.
[16] A. Thambidurai, J. K. Lourdusamy, J. V. John, S. Ganesan, Preparation and electrochemical behaviour of biomass based porous carbons as electrodes for supercapacitors - a comparative investigation, *Korean J. Chem. Eng.* **31** (2014) 268-275.
[17] L. Shi, L. Jin, Z. Meng, Y. Sun, C. Li, Y. Shen, A novel porous carbon material derived from the byproducts of bean curd stick manufacture for high-performance supercapacitor use, *RSC Adv.* **8** (2018) 39937.
[18] Y. S. Yun, M. H. Park, S. J. Hong, M. E. Lee, Y. W. Park, H. J. Jin, Hierarchically porous carbon nanosheets from waste coffee grounds for supercapacitors, *ACS Appl. Mater. Interfaces*. **7** (2015) 3684-3690.
[19] R. Farma, M. Deraman, A. Awitdrus, I. A. Talib, E. Taer, N. H. Basri, J. G. Manjunatha, M. M. Ishak, B. N. M. Dollah, S. A. Hashmi, Preparation of highly porous binderless activated carbon electrodes from fibres of oil palm empty fruit bunches for application in supercapacitors, *Bioresour. Technol.* **132** (2013) 254-261.
[20] N. H. Basri, M. Deraman, S. Kanwal, I. A. Talib, J. G. Manjunatha, A. A. Aziz, R. Farma, Supercapacitors using binderless composite monolith electrodes from carbon nanotubes and pre-carbonized biomass residues, *Biomass Bioenergy* **59** (2013) 370-379.
[21] N. S. M. Nor, M. Deraman, R. Omar, Awitdrus, R. Farma, N. H. Basri, B. N. M. Dolah, N. F. Mamat, B. Yatim, M. N. M. Daud, Influence of gamma irradiation exposure on the performance of supercapacitor electrodes made from oil palm empty fruit bunches, *Energy* **79** (2015) 183-194.
[22] N. S. M. Nor, M. Deraman, M. R. M. Jasni, J. G. Manjunatha, M. A. R. Othman, S. A. Shamsudin, Supercapacitors using binderless activated carbon monoliths electrodes consisting of a graphite additive and pre-carbonized biomass fibers, *Int. J. Electrochem. Sci.* **12** (2017) 2520-2539.
[23] V. Subramanian, C. Luo, A. M. Stephen, K. S. Nahm, S. Thomas, B. Wei, Supercapacitors from activated carbon derived from banana fibers, *J. Phys. Chem. C* **111** (2007) 7527-7531.
[24] L. Wang, G. Mu, C. Tian, L. Sun, W. Zhou, P. Yu, J. Yin, H. Fu, Porous graphitic carbon nanosheets derived from cornstalk biomass for advanced supercapacitors, *ChemSusChem* **6** (2013) 880-889.
[25] H. Jin, X. Wang, Y. Shen, Z. Gu, A high-performance carbon derived from corn stover via microwave and slow pyrolysis for supercapacitors, *J. Anal. Appl. Pyrol.* **110** (2014) 18-23.
[26] D. Wang, Z. Geng, B. Li, C. Zhang, High performance electrode materials for electric double-layer capacitors based on biomass-derived activated carbons, *Electrochim. Acta* **173** (2015) 377-384.
[27] M. Wahid, D. Puthusseri, D. Phase, S. Ogale, Enhance capacitance retention in a supercapacitor made of carbon from sugarcane bagasse by hydrothermal pretreatment, *Energ. Fuel* **28** (2014) 4233-4240.
[28] J. Liu, Y. Deng, X. Li, L. Wang, Promising nitrogen-rich porous carbons derived from one-step calcium chloride activation of biomass-based waste for high performance supercapacitors, *ACS Sustain. Chem. Eng.* **4** (2016) 177-187.
[29] T. Sesuk, P. Tammawat, P. Jivaganont, K. Somton, P. Limthongkul, W. Kobsiriphat, Activated carbon derived from coconut coir pith as high-performance supercapacitor electrode material, *J. Energ. Storage* **25** (2019) 100910–100919.
[30] J. Deng, M. Li, Y. Wang, Biomass-derived carbon: synthesis and applications in energy storage and conversion, *Green Chem.* **18** (2016) 4824–4854.
[31] T. F. Wang, Y. B. Zhai, Y. Zhu, C. T. Li, G. M. A. Zeng, Review of the hydrothermal carbonization of biomass waste for hydrochar formation: Process conditions, fundamentals, and physicochemical properties, *Renew. Sust. Energ. Rev.* **90** (2018) 223–247.
[32] P. Zhao, Y. Shen, S. Ge, K. Yoshikawa, Energy recycling from sewage sludge by producing solid biofuel with hydrothermal carbonization. *Energ. Convers. Manag.* **78** (2014) 815–821.
[33] Z. Liu, A. Quek, S. K. Hoekman, R. Balasubramanian, Production of solid biochar fuel from waste biomass by hydrothermal carbonization, *Fuel* **103** (2013) 943–949.

[34] A. Jain, C. Xu, S. Jayaraman, R. Balasubramanian, J. Y. Lee, M. P. Srinivasan, Mesoporous activated carbons with enhanced porosity by optimal hydrothermal pre-treatment of biomass for supercapacitor applications, *Microporous Mesoporous Mater.* **218** (2015) 55–61.

[35] M. E. Fernandez, B. Ledesma, S. Román, P. R. Bonelli, A. L. Cukierman, Development and characterization of activated hydrochars from orange peels as potential adsorbents for emerging organic contaminants, *Bioresour. Technol.* **183** (2015) 221-228.

[36] J. G. Lynam, C. J. Coronella, W. Yan, M. T. Reza, V. R. Vasquez, Acetic acid and lithium chloride effects on hydrothermal carbonization of lignocellulosic biomass, *Bioresour. Technol.* **102** (2011) 6192-6199.

[37] M. M. Titirici, A. Thomas, S. H. Yu, J. O. Müller, M. Antonietti, A direct synthesis of mesoporous carbons with bicontinuous pore morphology from crude plant material by hydrothermal carbonization, *Chem. Mater.* **19** (2007) 4205-4212.

[38] S. Song, D. Su, X. Xu, X. Yang, L. Wei, K. Li, G. Shao, Q. An, S. Zhai, N. Liu, Using citric acid to suppress lignin repolymerization in the organosolv pretreatment of corn stalk, *Ind. Crop Prod.* **200** (2023) 116881.

[39] N. A. M. Barakat, M. I. Osama, M. M. Hager, H_3PO_4/KOH Activation agent for high performance rice husk activated carbon electrode in acidic media supercapacitors, *Molecules* **28** (2023) 296.

[40] N. Zhou, H. Chen, Q. Feng, D. Yao, H. Chen, H. Wang, Z. Zhou, H. Li, Y. Tian, X. Lu, Effect of phosphoric acid on the surface properties and Pb(II) adsorption mechanisms of hydrochars prepared from fresh banana peels, *J. Clean. Prod.* **165** (2017) 221–230.

[41] S. W. Han, D. W. Jung, J. H. Jeong, E. S. Oh, Effect of pyrolysis temperature on carbon obtained from green tea biomass for superior lithium ion battery anodes, *Chem. Eng. J.* **254** (2014) 597-604.

[42] A. Stephan, T. Kumar, R. Ramesh, S. Thomas, S. Jeong, K. Nahm, Pyrolitic carbon from biomass precursors as anode materials for lithium batteries, *Mat. Sci. Eng. A. – Struct.* **430** (2006) 132-137.

[43] J. Figueiredo, Functionalization of porous carbons for catalytic applications, *J. Mater. Chem. A* **1** (2013) 9351-9364.

[44] C. Peng, X. B. Yan, R. T. Wang, J. W. Lang, Y. J. Ou, Q. J. Xue, Promising activated carbons derived from waste tea-leaves and their application in high performance supercapacitors electrodes, *Electrochim. Acta* **87** (2013) 401-408.

[45] I. K. Mbaraka, D. R. Radu, V. S. Y. Lin, B. H. Shanks, Organosulfonic acid-functionalized mesoporous silicas for the esterification of fatty acid, *J. Catal.* **219** (2003) 329-336.

[46] P. I. Ravikovitch, A. Vishnyakov, R. Russo, A. V. Neimark, Unified approach to pore size characterization of microporous carbonaceous materials from N_2, Ar, and CO_2 adsorption isotherms, *Langmuir* **16** (2000) 2311-2320.

[47] F. Chen, Y. Zhang, M. Zheng, Y. Xiao, H. Hu, Y. Liang, Y. Liu, H. Dong, Preparation of high-performance porous carbon materials by citric acid-assisted hydrothermal carbonization of bamboo and their application in electrode materials, *Energ. Fuel* **36** (2022) 9303–9312.

[48] S. Y. Lu, M. Jin, Y. Zhang, Y. B. Niu, J. C. Gao, C. M. Li, Chemically exfoliating biomass into a graphene-like porous active carbon with rational pore structure, good conductivity, and large surface area for high-performance supercapacitor, *Adv. Energ. Mater.* **8** (2018) 1702545.

[49] R. Demir-Cakan, N. Baccile, M. Antonietti, M. M. Titirici, Carboxylate-rich carbonaceous materials via one-step hydrothermal carbonization of glucose in the presence of acrylic acid, *Chem. Mater.* **21** (2009) 484–490.

[50] K. MacDermid-Watts, R. Pradhan, A. Dutta, Catalytic hydrothermal carbonization treatment of biomass for enhanced activated carbon: A review, *Waste Biomass Valorization* **12** (2021) 2171–2186.

[51] B. Liu, Y. Liu, H. Chen, M. Yang, H. Li, Oxygen and nitrogen co-doped porous carbon nanosheets derived from Perilla frutescens for high volumetric performance supercapacitors, *J. Power Sources* **341** (2017) 309–317.

[52] F. Huang, D. Chen, Towards the upper bound of electrochemical performance of ACNT@polyaniline arrays as supercapacitors. *Energ. Environ. Sci.* **5** (2012) 5833–5841.

[53] A. B. Mei, O. Munteshari, J. Lau, B. Dunn, L. Pilon, Physical interpretations of nyquist plots for EDLC electrodes and devices, *J. Phys. Chem. C* **122** (2018) 194-206.